1 Using Seismic Attributes in seismotectonic research: an application to
2 the Norcia's Mw=6.5 earthquake (30th October 2016) in Central Italy.

3 Maurizio Ercoli[1;4], Emanuele Forte[2], Massimiliano Porreca[1;4], Ramon Carbonell[3], Cristina Pauselli[1;4],
4 Giorgio Minelli[1;4], Massimiliano R. Barchi[1;4].
5
6 [1] Dip. di Fisica e Geologia – Università degli Studi di Perugia (Perugia, Italy).
7 [2] Dept. of Mathematics and Geosciences, University of Trieste (Trieste, Italy).
8 [3] Dept. Structure & Dynamics of the Earth, CSIC-Inst. Earth Sciences Jaume Almera (Barcelona, Spain).
9 [4] Member of Interuniversity Center for Research on 3D-Seismotectonics (Centro InterRUniversitario per l'Analisi
10 SismoTettonica tridimensionale con applicazioni territoriali – CRUST).

11 *Correspondence to*: Maurizio Ercoli (maurizio.ercoli@unipg.it; maurizio.ercoli@gmail.com)

12 **Abstract.** In seismotectonic studies, seismic reflection data are a powerful tool to unravel the complex deep architecture of

13 active faults. Such tectonic structures are usually mapped at surface through traditional geological surveying whilst seismic

14 reflection data may help to trace their continuation from the near-surface down to hypocentral depth. In this study, we

15 propose the application of the seismic attributes technique, commonly used in seismic reflection exploration by oil industry,

16 to seismotectonic research for the first time. The study area is a geologically complex region of Central Italy, recently struck

17 by a long-lasting seismic sequence including a Mw 6.5 main-shock. A seismic reflection data-set consisting of three vintage

18 seismic profiles, currently the only available across the epicentral zone, constitutes a singular opportunity to attempt a

19 seismic attribute analysis. This analysis resulted in peculiar seismic signatures which generally correlate with the exposed

20 surface geologic features, and also confirming the presence of other debated structures. These results are critical, because

21 provide information also on the relatively deep structural setting, mapping a prominent, high amplitude regional reflector

22 that marks the top basement, interpreted as important rheological boundary. Complex patterns of high-angle discontinuities

23 crossing the reflectors have been also identified. These dipping fabrics are interpreted as the expression of fault zones,

24 belonging to the active normal fault systems responsible for the seismicity of the region. This work demonstrates that

25 seismic attribute analysis, even if used on low-quality vintage 2D data, may contribute to improve the subsurface geological

26 interpretation of areas characterized by high seismic potential.

27 1 Introduction

28 Studying the connections between the earthquakes and the faults to which they are associated is a primary assignment of

29 seismotectonics (Allen et al., 1965; Schwartz and Coppersmith, 1984). Clearly, this is not an easy task: it is in fact generally

30 complex to fill the gap between the exposed geology including the active "geological faults" mapped by the geologists and

31   the seismic features describing the geometry and kinematics of the seismic source at hypocentral depth ("seismological

32   faults", e.g. Barchi & Mirabella, 2008).

33   In case of strong earthquakes, impressive topographic changes and surface ruptures are often reported (e.g. Press and

34   Jackson, 1965; Wyss & Brune, 1967; Jibson et al., 2018; Yi et al., 2018; Civico et al, 2018). While many studies on the

35   surface geology are generally performed, especially after important events, the recovery of deep information on the

36   seismogenic structures is always a challenge, primarily due to the lack of high-resolution geophysical data and/or wells

37   stratigraphy.

38   This fact generates uncertainties that may amplify the scientific debate and the number of models introduced by the

39   geoscientists. Therefore, this process requires the use of appropriate geophysical data, aimed at recovering information on

40   the deep geological architecture and, in particular, on the geometry of active faults.

41   Different geophysical methods (e.g. Gravimetry, Magnetics, Electric and Magnetotellurics, Ground Penetrating Radar) may

42   contribute to define the stratigraphy and structural setting of the upper crust at different scales. But the seismic reflection is

43   largely the most powerful tool producing high-resolution images fundamental to trace the actual geometry of active faults at

44   surface (usually mapped and reconstructed in geological cross-sections), from the near surface down to hypocentral depths.

45   However, the ex-novo acquisition of onshore deep reflection data, possibly 3D, is often hampered by environmental

46   problems, complex logistics, and high costs. These issues seriously limit the possible, widespread use of this technique for

47   scientific research. Significant exceptions are research projects for deep crustal investigations like BIRPS (Brewer et al.,

48   1983), CoCORP (Cook et al., 1979), ECORS (Roure et al., 1989) and CROP (Barchi et al., 1998; Finetti et al., 2001),

49   IBERSEIS (Simancas et al., 2003).

50   Such limitations can be partially overcome by considering old profiles (legacy data) acquired by the exploration industry.

51   When collected in seismically active regions, such data may be used to connect the active faults mapped at the surface with

52   the seismogenic sources depicted by seismological recordings (Boncio et al., 2000; Bonini et al., 2014; Carvalho et al., 2008;

53   Beidinger et al., 2011; Maesano et al., 2015; Porreca et al., 2018). Vintage profiles can therefore significantly contribute to

54   seismotectonic research, even if their location and orientation were not specifically designed with this aim. In addition,

55   seismic technologies and acquisition/processing strategies of some decades ago, produced data with both relatively low

56   signal/noise ratio (S/N) and resolution in comparison to modern data.

57   To improve the data quality and increase the accuracy of the interpretation, three main strategies can be usually considered:

58   1) collection of new reflection seismic data with modern technologies, optimizing feasibility studies on the base of available

59   vintage datasets; 2) reprocessing of the old data from raw to new stacks using new and available powerful capabilities and

60   developments and, 3) use post-stack processing techniques such as seismic attributes analysis. These approaches are

61   currently all used by the O&G industry (e.g. in the re-assessment of known reservoirs) and are clearly characterized by

62   different potential, costs and working time.

63   Some limitations characterize the first two approaches: the first is particularly demanding in terms of costs and logistic, and

64   not practicable in zones where the use of dynamite or arrays of vibroseis trucks is forbidden or limited (e.g. National Parks

65 or urban areas). The second requires broad projects encompassing specialized teams, high-computation power and generally

66 long processing times, the latter is dependent on the quality of the raw data. The third strategy, in the case of the attribute

67 analysis exploits a well-known and mature technique. It has been used since early 80's by the O&G exploration industry

68 (Chopra & Marfurt, 2005) for geometrical and petrophysical characterization of reservoirs (Chopra & Marfurt, 2008).

69 A seismic attribute is a quantity derived from seismic data (pre-stack and/or post-stack) that can be calculated on a single

70 trace, on multiple traces, or volumes. This technique is commonly used to extract additional information that may be unclear

71 in a traditional seismic image, therefore leading to a better interpretation of the data. Examples of applications on dense 3D

72 seismic volumes produced spectacular results (Chopra & Marfurt, 2007; Marfurt et al., 2011; Hale, 2013; Barnes, 2016,

73 Marfurt, 2018). Recent developments of approaches based on machine learning techniques are currently pushing it further to

74 contribute towards an objective (automatic) interpretation of seismic data-sets (Wrona et al., 2018; Di & AlRegib, 2019;

75 Naeini & Prindle, 2019). Therefore, among the three strategies, the attribute analysis is probably the easiest, cheapest and

76 fastest to qualitatively emphasize the geophysical features and data properties of reflection seismic data sets in complex

77 geological areas. Due to different well-known limitations and advantages existing between 2D vs 3D seismic data (these are

78 extensively discussed by Torvela et al. (2013) and Hutchinson (2016), 2D seismic attribute analysis of post-stack data may

79 be subjected to possible pitfalls and/or may not bring so impressive improvements in the seismic images. However, the main

80 point is that inland, most of the sedimentary basins have actually been sampled by 2D grids of seismic profiles, or at least

81 they have been probed by a few sparse 2D seismic lines. Hence, it is relevant to extract as much information as possible from

82 these 2D surveys in areas not covered by 3D seismic surveys. Whilst in the hydrocarbon industry this process is useful even

83 if mainly driven by a constant necessity to reduce the costs (Ha et al., 2019), in seismotectonic researches it is affected by

84 even worse limitations previously aforementioned. Therefore, also slight improvements obtained on vintage 2D data may

85 bring to new and unprecedent subsurface information in complex and active tectonic environments. We think that we might

86 successfully export a similar approach in a seismotectonic study applying this type of analysis on an active seismic zone,

87 covered only by a very limited number of 2D seismic lines. Based on such considerations, the selected study area is located

88 in the central Apennines (Central Italy), a region between the southeastern part of the Umbria-Marche Apennines and the

89 Laga Domain in the outer Northern Apennines (e.g. Barchi et al., 2001). This area presents ideal characteristics to test the

90 proposed new approach. In fact, in the past, several seismic profiles were acquired at this location for hydrocarbon

91 exploration, providing good constraints for subsurface geological interpretation (Bally et al., 1986; Barchi et al, 1991; Barchi

92 et al., 1998; Ciaccio et al., 2005; Pauselli et al., 2006; Mirabella et al. 2008; Barchi et al., 2009; Bigi et al., 2011). After the

93 last 2016-2017 seismic sequence, Porreca et al. (2018) have provided a new regional geological model based on the

94 interpretation of vintage 2D seismic lines. In such a study, the authors remark important differences in the seismic data

95 quality across the region. In fact, the eastern area that shows higher overall data quality, is located at the footwall of the

96 Mount Sibillini thrust (MSt) and, includes (consists of) flyschoid units of the Laga foredeep Domain. It is noteworthy that

97 the Mw 6.5 epicentral zone, is located on the MSt hanging-wall (Lavecchia, 1985). This is characterized by prevalent

98 carbonate sequence and, its crossed by seismic sections with lower S/N ratio, that hampered the subsurface interpretation.

99   Therefore, this contribution focuses on three low quality seismic cross-sections located close to the Mw 6.5 main-shock area,

100   aiming to exploit the use of seismic attributes to squeeze additional information. The main goal of this study is to obtain as

101   much information as possible on the geological structures responsible for the seismicity. Therefore, any improvement, that

102   for example can increase the resolution, the definition and/or the lateral continuity of the structural features is a very valuable

103   contribution. The current manuscript is an example of how can seismic attribute analysis contribute to seismotectonic

104   research as an innovative approach.

105   **2 Geological framework and seismotectonics of the study area**

106   During the 2016-2017, a wide part of Central Italy has been struck by a complex seismic sequence, characterized by multi-

107   fault ruptures occurred within few months (August 2016 – January 2017) similarly to previous seismic sequences in Central

108   Italy (e.g. L'Aquila and Colfiorito, Valoroso et al., 2013 and Chiaraluce et al., 2005). Nine earthquakes with M>5 and more

109   that 97'000 events in two years have been recorded at hypocentral depth not exceeding 12 km (Fig.1). The strongest

110   mainshock of Mw 6.5 occurred on 30th October 2016 (Chiaraluce et al., 2017; Chiarabba et al., 2018; Gruppo di Lavoro

111   Sequenza Centro Italia, 2019; Improta et al., 2019; ISIDe working group, 2019), generating impressive co-seismic ruptures

112   (Civico et al., 2018; Brozzetti et al., 2019).

113   The study area is located in the easternmost part of the Northern Apennines fold and thrust belt, including the Umbria-

114   Marche thrust and fold belt domain and Laga Formation. This is a geologically complex region, where in the past the

115   analysis of 2D seismic profiles have produced contrasting interpretation of the upper crust structural setting, e.g. thin vs.

116   thick skinned tectonics, fault reactivation/inversion, basement depth (Bally et al., 1986; Barchi, 1991; Barchi et al., 2001;

117   Bigi et al., 2011; Calamita et al., 2012; Porreca et al., 2018). The Umbria-Marche fold and thrust belt was formed during the

118   Miocene compressive phase, and overthrusts the Laga foredeep sequence, through arc-shaped major thrusts, namely the M.

119   Sibillini thrust (MSt, Koopman, 1983; Lavecchia, 1985), with eastward convexity. The compressional structures were later

120   disrupted by the extensional faults since the Late Pliocene.

121   The Umbria-Marche domain involves the rocks of the sedimentary cover, represented by three main units:

122   1) on top, the Laga sequence consisting of siliciclastic turbidites belonging to the Laga foredeep and foreland Formation

123   (Milli et al., 2007; Bigi et al., 2011); it is made by alternating layers of sandstones, marls and evaporites (Late Messinian –

124   Lower Pliocene, up to 3000 m thick, average seismic velocity (v_{av}) = 4000 m/s), mainly outcropping in the eastern sector of

125   the study area (i.e. at the footwall of the MSt).

126   2) in the middle, carbonate formations (Jurassic-Oligocene, about 2000 m thick, v_{av}= 5800 m/s) formed by pelagic

127   limestones (Mirabella et al., 2008) with subordinated marly levels overlying an early Jurassic carbonate platform (Calcare

128   Massiccio Fm.)

129   3) at the bottom, Late Triassic evaporites (1500–2500 m thick, v_{av}= 6400 m/s), consisting in alternated layers of anhydrites

130   and dolomites (Anidriti di Burano Fm. And and Raethavicula Contorta beds; Martinis & Pieri, 1964), never outcropping and

131 intercepted, only, by deep wells (Porreca et al., 2018 and references therein), representing the main ad deeper detachment of

132 the region.

133 An underlying basement of variable lithology (v_{av} = 5100 m/s) that never crops out (Vai, 2001), was intercepted by deep

134 wells (Bally et al., 1986; Minelli & Menichetti, 1990; Anelli et al., 1994; Patacca & Scandone, 2001) and, it is separated by

135 the aforementioned units by the aforementioned important regional decollement.

136 In a such complex structural setting, the Late Pliocene-Quaternary extensional tectonic phase, characterized by a prevalent

137 NE-SW stretching direction, produced NNW-SSE striking WSW-dipping normal faults. These faults were also responsible of

138 the tectono-sedimentary evolution of intra-mountain continental basins (Calamita et al., 1994; Cavinato and De Celles, 1999).

139 The most evident Quaternary basins of this part of the Apennines are the Castelluccio di Norcia (CNb) and Norcia (Nb) basins,

140 located respectively at 1270 and 700 m a.s.l. They have been subjected to a lacustrine and fluvial sedimentation of hundreds

141 of meters characterized by fine clayey to coarse grained deposits (Blumetti et al., 1993; Coltorti and Farabollini, 1995).

142 The area is affected by historical and instrumental seismicity with frequent small to moderate magnitude earthquakes (4 <

143 Mw < 7, Boncio and Lavecchia, 2000; Rovida et al., 2016). The recent 2016-2017 seismic sequence has been caused by the

144 activation of a complex NNW-SSE trending fault system, characterized by prevalent high-angle WSW-dipping normal faults

145 (Lavecchia et al., 2016). More in detail, the easternmost fault system of the region recently activated is the NNW-SSE

146 trending "Monte Vettore fault system" (Vf). This was the responsible of the mainshock nucleation between the continental

147 Norcia (Nb) and Castelluccio di Norcia basins (CNb) (Fig. 1). Nb and CNb are two asymmetrical grabens, bordered by high-

148 angle WSW-dipping normal faults located on their eastern flanks. Both fault systems are thought to have high seismogenic

149 potential and able to generate earthquakes up to Mw 7.0 (e.g. Barchi et al., 2000; Basili et al., 2008; Rovida et al., 2016;

150 DISS Working Group, 2018).

151 The Nb master fault (Nottoria-Preci fault, Nf) is considered responsible of the 1979 earthquake (Deschamps et al., 1984;

152 Brozzetti & Lavecchia, 1994; Rovida et al., 2016) and possibly associated to multiple historical events (Galli et al., 2005;

153 Pauselli et al., 2010; Galli et al., 2018), including the 1703 (Me = 6.8, Rovida et al., 2016). The CNb master fault (Vf) and its

154 secondary splays activated during the 2016-2017 sequence (e.g. Wilkinson et al., 2017; Villani et al., 2018a) were already

155 known and mapped due to paleo-seismological and shallow geophysical evidences (Galadini & Galli, 2003; Galli et al.,

156 2008; Ercoli et al., 2013; Ercoli et al., 2014). However, despite of the large amount of surface data collected (Livio et al.,

157 2016; Pucci at al., 2017; Wilkinson et al., 2017; De Guidi et al., 2017; Brozzetti et al., 2019; Galli et al., 2018), the deep

158 extension of the Norcia and Castelluccio faults (particularly the Vf) ,and the overall complex structure of the area are still

159 debated (Lavecchia et al., 2016; Porreca et al., 2018; Bonini et al., 2019, Cheloni et al., 2019, Improta et al. 2019).

3 Data

161 We have performed the seismic attributes analysis on three W-E trending 2D seismic reflection profiles crossing the

162 epicentral area between the Umbria and Marche regions (Central Italy, Fig.1). Such 2D data are part of a much larger,

163 unpublished dataset including 97 seismic profiles and few boreholes, drilled for hydrocarbon exploration by ENI in the

164 period 1970-1998.

165 The data quality is extremely variable (medium/poor) with limited fold (generally < 60 traces / Common Mid-Point - CMP)

166 mainly due to environmental and logistical factors like: acquisition technologies, limited site access, complex tectonic

167 setting, and different (contrasting) outcropping lithologies like Carbonates and Quaternary sediments that resulted often in

168 low S/N recordings (e.g. Mazzotti et al., 2000, Mirabella et al., 2008).

169 The analysed lines include: NOR01 (stack, 14 km long), NOR02 (time-migrated, 20 km long, partially parallel to NOR01 on

170 the western sector), and CAS01 (stack, 16 km long), located more to the south (Fig. 1). NOR01 and CAS01 were acquired

171 using a Vibroseis source, whilst explosive was used for NOR02; all the lines are displayed in Two-Way-Travel-Time

172 (TWTT) limited to 4.5 s. The average frequency spectra display bandwidths ranging from few Hz up to 60-70 Hz, whilst

173 NOR02 extends up to 100 Hz. Assuming the average peak frequency of 20 Hz, a vertical resolution of ca. 80 m can be

174 estimated (average carbonate velocity = 6 km/s, parameters in Table 1s, supporting information). Some processing artefacts

175 (A) are visible in NOR01 as a straight horizontal signal at ca. 1 s (Fig. 2a), and two others sub-horizontal between 1-2 s in

176 CAS01 (Fig. 1s-a, supporting information). However, some seismic events and lineaments, related to geological structures of

177 interest, are slightly visible and their display seems potentially improvable with a proper choice of seismic attributes type

178 and parameters. Therefore, we loaded the lines into the OpendTect (OdT) software, setting up a common seismic datum

179 equal to 500 m while adding some ancillary data, extracted by a complementary GIS (QGis software) project including:

180 regional fault patterns (from maps and Ithaca database), a regional DTM (Tarquini et al., 2007; Tarquini et al., 2012),

181 geological maps (Pierantoni et al., 2013; Carta Geologica Regionale 1:10'000 – Regione Marche, 2014; Carta Geologica

182 Regionale 1:10'000 – Regione Umbria, 2016), as well as mainshock earthquakes distribution belonging to the studied

183 seismic sequence (Iside database). The integration of such information in a pseudo-3D environment offered us a

184 multidisciplinary platform to clearly display the seismic lines and to link surface data and the deep geologic structures at

185 hypocentral depth.

186 **4 Methods**

187 The seismic reflection data interpretation is generally accomplished through the definition of specific signal characteristics

188 (seismic signature), supported by the geological knowledge of the study area. A standard seismic interpretation is affected by

189 a certain degree of uncertainty/subjectivity (particularly in case of poor data quality), because generally based on a

190 qualitative analysis of reflection amplitude, geometry and lateral continuity. Over the last years, the introduction of seismic

191 attributes and related automated/semi-automated procedures had an important role in reducing the subjectivity of seismic

192 interpretation, at first in 2D/3D seismic reflection data (Barnes 1996; Taner et al., 1979; Barnes, 1999; Chen and Sidney,

193 1997; Taner, 2001; Chopra and Marfurt, 2007; Chopra and Marfurt, 2008; Forte et al., 2016) and, more recently, also in

194 other reflection techniques like the Ground Penetrating Radar (GPR) (e.g. McClymont et al., 2008; Forte et al., 2012; Ercoli

195 et al., 2015, De Lima et al., 2018). In this work, we have tested several post-stack attributes on three 2D vintage seismic

196   lines, also using composite multi-attribute displays. Among those analysed, we selected the three attributes that resulted in

197   the best images, making possible to detect peculiar seismic signatures of regional seismogenic layers and fault zones. Details

198   about the calculated attributes are hereafter provided.

199

200   **"Energy" (E):** one of the RMS amplitude-based attributes, it is defined as the ratio between the squared sum of the

201   sample values in a specified time-gate and the number of samples in the gate (Taner, 1979, Chopra & Marfurt,

202   2005, Chopra & Marfurt, 2007). The Energy measures the reflectivity in a specified time-gate, so the higher the

203   Energy, the higher is the reflection amplitude. In comparison to the original seismic amplitude, it is independent of

204   the polarity of the seismic data being always positive, and in turn preventing the zero-crossing problems of the

205   seismic amplitude (Forte et al., 2012, Ercoli et al., 2015, Lima et al., 2018, Zhao et al., 2018). This attribute is

206   useful to emphasize the most reflective zones (e.g. characterization of acoustic properties of rocks). It may also

207   enhance sharp lateral variations in seismic events, highlighting discontinuities like fractures and faults. In this work,

208   we set a 20 ms time window (i.e. about the mean wavelet length), obtaining considerable improvements in the

209   visualization of higher acoustic impedance contrasts.

210   **"Energy gradient" (EG):** it is the first derivative of the energy with respect to time (or depth). The algorithm

211   calculates the derivative in moving windows and returns the variation of the calculated energy as a function of time

212   or depth (Chopra & Marfurt, 2007; Forte et al., 2012). It is a simple and robust attribute, also useful for a detailed

213   semi-automatic mapping of horizons with a relative low level of subjectivity. The attribute acts as an edge detection

214   tool, effective in the mapping of the reflection patterns as well as the continuity of both steep discontinuities like

215   faults and fractures, and channels, particularly in slices of 3D data (Chopra & Marfurt, 2007). In this work, we have

216   used the same time window of the Energy, obtaining considerable improvements in the visualization not only of the

217   strong acoustic impedance reflectors but particularly in the faults imaged in the shallowest part of the seismic

218   sections.

219   **Pseudo-relief (PR):** it is obtained in two steps: the energy attribute is first computed in a short time window, then

220   followed by the Hilbert transform (phase rotation of -90 degrees). The Pseudo-relief is considered very useful in 2D

221   seismic interpretation to generate "outcrop-like" images allowing an easier detection of both faults and horizons

222   (Bulhões, 1999; Barnes et al., 2011; Vernengo et al. 2017, Lima et al., 2018). In this work, considerable display

223   improvements have been obtained using the Pseudo-relief computed in a window of 20 ms. In comparison to the

224   standard amplitude, it better highlights the reflection patterns and thus the continuity/discontinuity of reflectors,

225   enhancing steep discontinuities and fault zones.

226   **5 Results**

227   The comparison between the original seismic lines and the images obtained after the attribute analysis allows to detect

228   considerable improvements in the visualization and interpretability of the geophysical features. In profiles NOR01, CAS01

229   and NOR02 (Figs 2, 3 and 4, respectively) we focus our analysis on three main types of geophysical features highlighted by

230   the attributes: sub-horizontal deep reflectors, low-angle and high-angle discontinuities.

231   Analysing in detail the line NOR01 (Fig. 2a, line location in the excerpt on the top), the most apparent low-angle

232   geophysical features are located in the eastern portion of the line between 2-3 s of the time window. The EN attribute in Fig.

233   2b clearly enhances a high-amplitude, gently W-dipping event at about 2.5 s (blue arrows). The EG and SR attributes of

234   NOR01 show clearly that this horizon (Figs. 2c, 2d, hereafter H) is characterized by a continuous package of reflectors (ca.

235   200 ms in TWT, ca. 8 km long), with common characteristics in terms of reflection strength and period.

236   A similar feature showing such a peculiar signature is visible also in CAS01, approximately at the same time interval (Fig.

237   3a, line location reported on the top insert). But in comparison to NOR01, it appears more discontinuous all along the

238   seismic profile, and in addition it is partially interfering with suspicious processing artefacts (highlighted with yellow dots,

239   labelled as "A", slightly undulated in Fig. 3a whilst horizontal in Fig. 2a ca. at 1 s). For those reasons, H is not particularly

240   clear in the standard amplitude line CAS01 (Fig. 3a), even if it is mainly visible on the westernmost side and beneath the

241   southern termination of Nb (ca. between 11-15 km). Despite a generalized high frequency noise content, H is better

242   enhanced in fig. 3b by EN attribute (blue arrows), and in particular by the EG and PR attributes (Figs. 3c and 3d), that

243   considerably help to better detect and mark its extension and geometry.

244   Regarding the most visible steep geophysical features detectable in these two seismic profiles, in NOR01 a high-angle E-

245   dipping lineament is defined by a clear high-angle discontinuity of the seismic signal, particularly enhanced in the eastern

246   sector (distance ca. 10 km) below the Nb (red arrows in fig. 2c and 2d). A very similar high-angle East-dipping discontinuity

247   can be noticed in the eastern sector of CAS01 (red arrows in Fig. 3c and 3d). Another main high-angle W-dipping lineament

248   is enhanced in Figs. 2c-2d of NOR01 (red arrows at the end of the line), that clearly divides two patterns of reflectors

249   showing different dip; this discontinuity propagates down to ca. 2.5 s and intercepts the aforementioned strong reflector H.

250   Between those two main alignments bounding the Nb, other similar but minor discontinuities can be also noticed crossing

251   and slightly disrupting the shallower reflectors: those high angle features are efficiently displayed by the EG and PR

252   attributes (Fig. 2c, 2d), whilst in the original line in Fig. 2a cannot be really appreciated.

253   The figure 4a display the original seismic line NOR02 characterized by similar geophysical features (location on the top

254   insert). The EN attribute in Fig. 4b again results efficient in enhancing sub-horizontal (blue arrows) and also gently dipping

255   deep events (green dots). On the western sector, the attributes in Figs. 4b and 4c show a pattern of relatively continuous and

256   gently W-dipping events between 0-2.5 s (0-5 km along the line). The most evident high-amplitude and continuous reflector

257   characterizes the central part of NOR02 at ca. 3.2–3.5 s (blue arrows in Figs. 4b, 4c, 4d), gently East-dipping and relatively

258   continuous for more than 8 km. This latter is intercepted by an important and well visible low-angle W-dipping discontinuity

259   (T, green dots in Figs. 4b, 4c and 4d). It crosses the entire profile, rising from about 4 s (West) to ca. 2 s (East), where it

260   intercepts one of the high amplitude events on the eastern end of the seismic line (18-20 km). Here again the attribute

261   analysis results extremely efficient to clearly detect such geophysical features otherwise poorly visible on the original line

262   NOR02 in Fig. 4a.

263   The most important result provided by the EG and PR attributes is a much clear visualization of the reflection patterns of

264   NOR02, aiding an easier detection of high-angle discontinuities, at different scales. In fact, a main high-angle E-dipping

265   discontinuity (red arrows) delimits the NOR02 western sector (ca. 1 km of distance along the line at surface); another steep

266   W-dipping alignment (red arrows) clearly cuts and slightly disrupt the set of reflectors below the Nb (0-2.5 s, ca. 4-5 km). In

267   addition, smaller discontinuities pervasively cross-cut the set of reflectors between 1-4 km bounded by such two main

268   features, producing a densely fragmented reflectors pattern in the middle portion. Another steep E-dipping feature is visible

269   at higher depth (red arrows at 1-3 s, ca. 7-9 km) beneath the topographic relief separating Nb by CNb: it seems to end up on

270   the deep surface T and in addition it doesn't reach the shallower portion of the seismic line. This discontinuity is subparallel

271   to a similar structure displayed in a more central portion of NOR02 (western side of CNb highlighted by red arrows at 10-12

272   km). The Figs. 4c and 4d show here sets of reflectors sharply interrupted, fragmented and displaced in a narrow zone. The

273   same seismic pattern is present in the western side of CNb, but it is due to some west-dipping discontinuities located

274   between 14-16 km. These features highlight an asymmetric "V-shape" fabric characterized by very short and fragmented

275   reflectors bounded by those two steep features of opposite dip. The deep continuation of such a main W-dipping alignment

276   also seems to truncate and disrupt both the gently-dipping discontinuity T and the deep reflector H: at approximately 3.2 s, it

277   appears interrupted laterally on its western side (Figs. 4c and 4d).

278   The results of this work produced has globally improved the interpretability of the original dataset. In particular, the data

279   integration in a 3D environment and the use of multi-attribute displays clarified the deep geometries of the main reflectors

280   and of the geophysical discontinuities, later interpreted on the light of the known and debated tectonic structures on the study

281   area. This is particularly clear in Fig. 5a, in which we report the seismic line NOR02 after the combined plot of the PR

282   attribute ("similarity" palette) with superimposed the EG attribute ("energy" palette), overlapped using ODT software (depth

283   conversion with V_{Pav} = 6000 m/s, vertical scale 2x). The reflectors characteristics and the discontinuities are clearly visible at

284   different levels of detail, and the two boxes (blue and black colours, respectively) highlight on the two most representative

285   seismic facies described before. The blue box of Fig.5a is reported in Fig. 5b and 5c by displaying a comparison of the H

286   signature in the original line and a plot of the EN attribute superimposed on the PR attribute. On the two other inserts in Figs.

287   5d and 5e, the same comparison of the data included in the black box is proposed. Fig.4d shows the scarce detectability of

288   the dense pattern of steep discontinuities in the original seismic profile (SA). The Fig.5e displays the enhancement obtained

289   plotting the PR attribute ("similarity palette") in transparency on the seismic line in amplitude (SA).

290   An analogous visualization is proposed in Fig. 6a for the seismic line NOR01. The comparison between the multi-display of

291   attributes PR and EG (blue box in Fig. 6a), the original line (Fig. 6b) and the EN+PR plot (Fig.6c) shows the improved

292   signature of the strong reflector H. The black box again reports the original line NOR01 and the version PR+SA, clearly

293   boosting the visualization of the high-angle discontinuities.

294   Such results therefore ensure an easier and more accurate interpretation of the subsurface geological structures; those are

295   connected with the surface geology and related to the hypocentre location of the main seismic events, that will be discussed

296   more in detail within the following chapter.

6 New constraints on the deep geological structure reconstruction

Due to the lack of 3D seismic volumes and of a regular grid of 2D seismic profiles in the area, the geological meaning of the results provided by the attributes analysis have been constrained by integrating all the other available literature data. We have therefore integrated geological and structural maps (Koopman, 1983; Centamore et al., 1993; Pierantoni et al., 2013), high-resolution topographic data (Tarquini et al., 2007 and 2012), mainshocks hypocentral data (Chiaraluce et al., 2017) and co-seismic surface ruptures data (Civico et al., 2018; Villani et al., 2018; Brozzetti et al., 2019).

In fig. 7, a 3D overview of the study region summarizes the data analysed across the area surrounding the Mw 6.5 mainshock (30th October 2016), plotter together with other three strong seismic events in the Northern sector. The two seismic images in Figs. 7b and 7c have been obtained by using again a multi-attributes visualization, in this case overlapping the PR and EN attributes in transparency with the original seismic lines NOR01 and NOR02. The black boxes centred on the NB and CNb basins have been magnified above and display the limits of the bounding faults (black dashed lines) and the main important reflectors detected in depth. In the Figs. 7d and 7e, we propose a detailed interpretation of the geophysical features displayed by the attribute images, together with the location of the focal mechanisms of the principal mainshocks.

The deep, high-amplitude reflector (H, blue arrows and dashed line) highlighted to the West of Nb in NOR01 (at 2.5 s, in Figs. 2d and 7d and in Figs. 3d of CAS01), presents an attribute signature similar to the one deeper visible in NOR02 beneath CNb (3.2 s, in Figs. 4b and 7e). This set of reflectors are interpreted as a high acoustic impedance contrast, possibly related to an important velocity inversion occurring between the Triassic Evaporites (anhydrites and dolostones, $Vp \approx 6$ km/s, e.g. Trippetta et al., 2010) and the underlying acoustic Basement (metasedimentary rocks, $Vp \approx 5$ km/s, sensu Bally et al., 1986). Similar, prominent reflections were detected in adjacent regions of the Umbria-Marche Apennines (e.g. Mirabella et al., 2008) confirming its regional importance, particularly because it represents a lithological control marking a seismicity cutoff (Porreca et al., 2018; Mancinelli et al., 2019).

The continuity of the deep reflector H is interrupted in the western edge by the low-angle west-dipping T discontinuity crossing NOR02 (Figs. 4d and 7e), not identified by Porreca et al. (2018). We interpret this discontinuity as the evidence of a deep thrust emerging in the easternmost sector of the region.

The steep discontinuities highlighted by the attribute analysis are here interpreted as the seismic signature at depth of complex normal faults mapped at the surface. More in detail, the most evident seismic discontinuity is marked by an E-dipping fault in NOR01, bordering westward the Nb (Figs. 2d and 7d). The latter does not have a clear surface expression and therefore its presence is still debated in literature (Blumetti et al., 1993; Pizzi et al., 2002; Galadini et al., 2018; Galli et al., 2018): its location and geometry in NOR01 perfectly match the supposed position at surface. Therefore, it may represent the evidence of the antithetic normal fault of Norcia (aNf), belonging to a conjugate tectonic system (Brozzetti & Lavecchia, 1994; Lavecchia et al., 1994) and suggested by morphological evidences (Blumetti et al., 1990) and paleoseismological records (Borre et al., 2003). It is a synthetic (W-dipping) high-angle, normal fault bordering the eastern flank of Nb ("Nottoria-Preci fault" – Nf, Calamita et al., 1982; Blumetti et al., 1993; Calamita & Pizzi, 1994). The Nf in NOR02 is

330   evident by a downward propagation of steep alignments (red arrows, Figs. 2c, 2d and 7d), that generates sharp lateral

331   truncations of the gently W-dipping reflectors. This area is also fragmented by several minor strands parallel to the main

332   faults (Figs. 7d). In addition, another similar structure is visible slightly eastward (Figs.4c, 4d red arrows between 7-9 km,

333   ca. 1-3 s and westernmost dashed black line in Fig. 7e). It is not reaching the shallower portion of the seismic line, but it is

334   clearly visible in depth down to the discontinuity T. This feature might be interpreted as a parallel E-dipping fault, moreover

335   suggested by several authors to be connected with an aftershock (Mw5.4), that "ruptured a buried antithetic normal fault on

336   eastern side of Nb, parallel to the western bounding fault of CNb" (Chiaraluce et al., 2017, Porreca et al., 2018 and Improta

337   et al., 2019).

338   The central sector of NOR02 including CNb, was described as a "triangle-shaped zone" by Porreca et al. (2018), who remark

339   a generalized difficulty to detect the accurate position of the normal faults. The multi-attribute visualization shows a clear

340   reflection fabric dominated by high-angle discontinuities. Those are interpretable as two opposite dipping normal faults

341   bordering the basin, well matching their positions mapped at surface (cfr. Pierantoni et al., 2013).

342   The main fault is here represented by the W-dipping Vf fault, reactivated during the 2016 earthquake (Villani et al., 2018a).

343   It can be traced, from its surface expression downward to hypocentre location along its deep seismic signature, made by

344   several high-angle seismic discontinuities cross-cutting the gently W-dipping reflectors (Figs. 4d and 7e). At depth, the Vf

345   seems also to displace the Top Basement (H) and the thrust (T) at about 3.2 s.

346   Analogous considerations can be extended to the E-dipping set of steep events at the westward side of CNb. These may

347   represent evidence of an antithetic fault (aVf), made by several minor fault strands (Villani et al., 2018b). Such a fault

348   appears connected at about 2-3 s to the W-dipping master Vf, producing a geometry of a conjugate system similar to Nb

349   (Figs. 4d and 7e).

350   For both Nb and CNb, the interpreted data suggest two slightly asymmetric fault systems, due to conjugate sets of

351   seismogenic master faults (Ramsay & Huber, 1987) producing a "basin-and-range" morphology (Serva at al., 2002). Those

352   control the evolution of the continental basins, and are associated with several complex sets of secondary strands, able to

353   produce surface ruptures as occurred in the 2016-2017seismic swarm.

354   The attribute images produced in this work suggest that such synthetic and antithetic tectonic structures at the Nb and CNb

355   cannot be actually simplified as a unique fault plane, but as complex and fractured fault zones (Fz, in Fig. 7d), like also

356   conceived also by Ferrario & Livio (2018) as "distributed faulting and rupture zones".

Conclusions

358   Taking into account the important role that seismic attributes play in the O&G industry their usage might be similar interest

359   for seismotectonic studies. And have a high potential impact on earthquakes hazard assessment.

360   This contribution presents one of the first case studies where the seismic attribute analysis is used for seismotectonic purposes.

361   The analysis is applied to seismic reflection data collected more than 30 years ago in Central Italy. Such industrial data,

362   nowadays irreproducible in regions where the seismic exploration is forbidden, represent, despite the limited quality, a unique

363   high-resolution source of information.

364   This contribution reveals that the use of seismic attributes can greatly improve the interpretation for the subsurface assessment

365   and structural characterization. Certainly, the overall low quality of the data sets did neither allow to extract rock petrophysical

366   parameters, nor more quantitative information. However, the attributes aid the seismic interpretation to better display the

367   reflection patterns of interest and provided new and original details on complex tectonic region in Central Italy. We

368   considerably improved the overall interpretability of the vintage seismic lines crossing the epicentral area of the 2016-2017

369   Norcia-Amatrice seismic sequence. In particular, we detected peculiar seismic signatures of a deep horizon of regional

370   importance, corresponding, most probably, to the base of the seismogenic layer, and to the location and geometry of the

371   complex active fault zones. Those consists of several secondary synthetic and antithetic splays in both the Quaternary basins,

372   generally consistent with its surface location, but also reinforcing the existence of faults with no clear surface outcrop, issue

373   currently much debated in the literature.

374   The analysis and integration of the seismic attributes has allowed the determination of the deep continuation of the (known

375   and supposed) faults and, the recently mapped co-seismic ruptures at surface, providing a pseudo-3D picture of the buried

376   structural setting of the area. The seismic attributes may help to reduce the gap between the surface geology and deep

377   seismological data, also revealing, a high structural complexity at different scales, that cannot generally be detected by using

378   only traditional interpretation techniques.This approach has shown the potential of the attributes analysis , that even when

379   applied on 2D vintage seismic lines, may significantly extend the data value. For all these reasons, we strongly encourage its

380   application for seismotectonic research to provide new information and additional constraints across other seismically active

381   regions around the world.

Acknowledgments

383   We are grateful to Eni S.p.A. for providing an inedited set of seismic reflection lines after the 2016-2017 seismic crisis in
384   Central Italy (raw data available in Fig.2 of supporting information). The original seismic reflection lines used in this study
385   are available in the supplementary material, well as the high-resolution Figures 2,3,4,7. The authors are very grateful to dgB
386   Earth Sciences and to QGIS team for providing the academic software used in this work. We thank Dr. Christian Berndt for
387   his useful comments in the revision of the paper.

References

Allen, C. R., St. Amand, P., Richter, C. F., & Nordquist, J.: Relationship between seismicity and geologic structure in the southern California region. Bulletin of the Seismological Society of America, 55(4), 753-797, 1965.

Anelli, L., Gorza, M., Pieri, M., and Riva, M.: Subsurface well data in the Northern Apennines (Italy). Memorie della Società Geologica Italiana, 48, 461–471, 1994.

Bally, A. W., Burbi, L., Cooper, C., & Ghelardoni, R.: Balanced cross-sections and seismic reflection profiles across the central Apennines. Memorie della Societa Geologica Italiana, 35, 257–310, 1986.

Barchi, M.: Integration of a seismic profile with surface and subsurface geology in a cross-section through the Umbria-Marche Apennines. Bollettino della Società Geologica Italiana, 110, 469–479, 1991.

Barchi, M. R., Minelli, G. and Pialli, G.: The CROP 03 Profile: a synthesis of results on deep structures of the Northern Apennines, Mem. Soc. Geol. It., 52, 383-400, 1998.

Barchi M.R., Galadini, F., Lavecchia, G., Messina, P., Michetti, A. M., Peruzza, L., Pizzi, A., Tondi & Vittori, E.: Sintesi delle conoscenze sulle faglie attive in Italia Centrale: parametrizzazione ai fini della caratterizzazione della pericolosità sismica. CNR-Gruppo Nazionale per la Difesa dai Terremoti, Roma, 62 pp., 2000.

Barchi, M., Landuzzi, A., Minelli, G., & Pialli, G.: Outer northern Apennines. In anatomy of an orogen: The Apennines and adjacent Mediterranean Basins. Netherlands, Springer, 215–253, 2001.

Barchi, M. R., & Mirabella, F.: The 1997-98 Umbria-Marche earthquake sequence: "Geological" vs. "seismological" faults. Tectonophysics, 476(1–2), 170–179. https://doi.org/10.1016/j.tecto.2008.09.013, 2009.

Barnes, A. E.: Theory of two-dimensional complex seismic trace analysis. Geophysics, 61, 264–272, 1996.

Barnes, A. E.: Attributes for automating seismic facies analysis. Seg Technical Program Expanded Abstracts, 19. doi:10.1190/1.1816121, 1999.

Barnes, A. E.: "Displaying Seismic Data to Look Like Geology", chapter of: "Attributes: New Views on Seismic Imaging– Their Use in Exploration and Production", Marfurt, K. J. Gao, D., Barnes, A., Chopra, S., Corrao, A., Hart, B., James, H., Pacht, J., Rosen, N.C. (2011), SEPM Society for Sedimentary Geology, 31, doi: 10.5724/gcs.11.31, 2011.

Barnes, A., E.: Handbook of Poststack Seismic Attributes, Society of Exploration Geophysicists, 21, doi: 10.1190/1.9781560803324, 2016.

Basili, R., Valensise, G., Vannoli, P., Burrato, P., Fracassi, U., Mariano, S., ... & Boschi, E.: The Database of Individual Seismogenic Sources (DISS), version 3: summarizing 20 years of research on Italy's earthquake geology. Tectonophysics, 453(1-4), 20-43, 2008.

Beidinger, A., Decker, K., & Roch, K. H.: The Lassee segment of the Vienna Basin fault system as a potential source of the earthquake of Carnuntum in the fourth century AD. International Journal of Earth Sciences, 100(6), 1315-1329, 2011.

Bigi, S., Casero, P., & Ciotoli, G.: Seismic interpretation of the Laga basin; constraints on the structural setting and kinematics of the central Apennines. Journal of the Geological Society, 168(1), 179–190. doi 10.1144/0016-76492010-084, 2011.

421 Borre, K., Cacon, S., Cello, G., Kontny, B., Likke Andersen, H., Moratti, G., Piccardi, L., Stemberk, J., Tondi, E., Vilimek,
422 V.: The COST project in Italy: analysis and monitoring of seismogenic faults in the Gargano and Norcia areas (centralsouthern
423 Apennines, Italy). J. Geodyn. 36, 3 –18, 2003.

424 Blumetti, A.M., Coltorti, M., Dramis, F., Farabollini, P.: Due sezioni stratigrafiche nel Pleistocene medio della conca di Norcia;
425 implicazioni geomorfologiche e neotettoniche. Rend. Soc. Geol. Ital. 13, 17– 26, 1990.

426 Blumetti, A. M., Dramis, F., & Michetti, A. M.: Fault-generated mountain fronts in the central Apennines (Central Italy):
427 Geomorphological features and seismotectonic implications. Earth Surface Processes and Landforms, 18(3), 203–223. doi:
428 10.1002/esp.3290180304, 1993.

429 Bonini, L., Toscani, G., & Seno, S.: Three-dimensional segmentation and different rupture behavior during the 2012 Emilia
430 seismic sequence (Northern Italy). Tectonophysics, 630, 33-42, 2014.

431 Bonini, L., Basili, R., Burrato, P., Cannelli, V., Fracassi, U., Maesano, F. E., et al.: Testing different tectonic models for the
432 source of the Mw 6.5, 30 October 2016, Norcia earthquake (central Italy): A youthful normal fault, or negative inversion of
433 an old thrust? Tectonics, 38, doi:10.1029/2018TC005185, 2019.

434 Boncio, P., F. Brozzetti, and G. Lavecchia: Architecture and seismotectonics of a regional low-angle normal fault zone in
435 central Italy, Tectonics, 19(6), 1038–1055, doi:10.1029/2000TC900023, 2000.

436 Boncio, P., Lavecchia, G., & Pace, B.: Defining a model of 3D seismogenic sources for seismic hazard assessment applications:
437 The case of central Apennines (Italy). Journal of Seismology, 8(3), 407–425, 2004.

438 Brewer, J. A., Matthews, D. H., Warner, M. R., Hall, J., Smythe, D. K., & Whittington, R. J.: BIRPS deep seismic reflection
439 studies of the British Caledonides. Nature, 305(5931), 206, 1983.

440 Brozzetti, F., & Lavecchia, G.: Seismicity and related extensional stress field: the case of the Norcia seismic zone. Annales
441 Tectonicae, 8, 38–57, 1994.

442 Brozzetti, F., Boncio, P., Cirillo, D., Ferrarini, F., de Nardis, R., Testa, A., Liberi, F., & Lavecchia, G.: High resolution field
443 mapping and analysis of the August – October 2016 coseismic surface faulting (Central Italy Earthquakes): slip distribution,
444 parameterization and comparison with global earthquakes. Tectonics, 38. https://doi.org/10.1029/2018TC005305, 2019.

445 Bulhões, E.M.: Técnica "Volume de Amplitudes". SBGF/6° Congresso Internacional da Sociedade Brasileira de Geofísica,
446 Rio de Janeiro, Anais (In Portuguese), 1999.

447 Calamita, F., Coltorti, M., Deiana, G., Dramis, F. and Pambianchi, G.: Neotectonic evolution and geomorphology of the Cascia
448 and Norcia depressions (Umbria-Marche Apennines), Geografia Fisica e Dinamica Quaternaria, 5, 263-276, 1982.

449 Calamita, F., & Pizzi, A.: Recent and active extensional tectonics in the southern Umbro-Marchean Apennines (Central Italy).
450 Memorie della Società Geologica Italiana, 48, 541–548, 1994.

451 Calamita, F., Pace, P., & Satolli, S., Coexistence of fault-propagation and fault-bend folding in curve-shaped foreland fold-
452 and-thrust belts: examples from the Northern Apennines (Italy). Terra Nova, 24(5), 396-406, 2012.

453 Carvalho, J., Taha, R., Cabral, J., Carrilho, F. and Miranda, M.: Geophysical characterization of the OtaVila Franca de Xira-
454 Lisbon-Sesimbra fault zone, Portugal. Geophysical Journal International, 174, 567-584, 2008.

455 Cavinato, G. P., & De Celles, P. G.: Extensional basins in the tectonically bimodal central Apennines fold-thrust belt, Italy:
456 Response to corner flow above a subducting slab in retrograde motion. Geology, 27(10), 955–958, 1999.

457 Centamore, E., Adamoli, L., Berti, D., Bigi, G., Bigi, S., Casnedi, R., et al.: Carta geologica dei bacini della Laga e del Cellino
458 e dei rilievi carbonatici circostanti. In: Studi Geologici Camerti, Vol. Spec. Università degli Studi, Dipartimento di Scienze
459 della Terra. SELCA, Firenze, 1992.

460 Cheloni, D., Falcucci, E., & Gori, S.: Half-graben rupture geometry of the 30 October 2016 MW 6.6 Mt. Vettore-Mt. Bove
461 earthquake, central Italy. Journal of Geophysical Research: Solid Earth, 124. https://doi.org/10.1029/2018JB015851

462 Chen, Q. and Sidney, S.: Seismic Attribute Technology for Reservoir Forecasting and Monitoring. The Leading Edge, 16 (5):
463 445. http://dx.doi.org/10.1190/1.1437657, 1997.

464 Chiarabba, C., De Gori, P., Cattaneo, M., Spallarossa, D., & Segou, M.: Faults geometry and the role of fluids in the 2016–
465 2017 Central Italy seismic sequence. Geophysical Research Letters, 45, 6963–6971, 2018.

466 Chiaraluce, L., Barchi, M., Collettini, C., Mirabella, F. & Pucci, S. Connecting seismically active normal faults with
467 Quaternary geological structures in a complex extensional environment: the Colfiorito 1997 case history (northern Apennines,
468 Italy). Tectonics 24, TC1002, https://doi.org/10.1029/2004TC001627, 2005.

469 Chiaraluce, L., Di Stefano, R., Tinti, E., Scognamiglio, L., Michele, M., Casarotti, E., et al.: The 2016 Central Italy seismic
470 sequence: A first look at the mainshocks, aftershocks, and source models. Seismological Research Letters, 88(3), 757–771.
471 https://doi.org/10.1785/0220160221, 2017.

472 Chopra, S. & J. Marfurt, K.: Seismic attributes - A Historical Perspective. Geophysics. 70(5):3.
473 https://doi.org/10.1190/1.2098670, 2005.

474 Chopra, S. and Marfurt, K. J.: Seismic Attributes for Prospect Identification and Reservoir Characterization. SEG Geophysical
475 Developments Series No. 11, Stephen J. Hill, series editor and volume editor. ISBN 978-1-56080-141-2 (volume) - ISBN 978-
476 0-931830-41-9 (series), 464 pp, 2007.

477 Chopra, S. & J. Marfurt, K.: Emerging and future trends in seismic attributes. The Leading Edge. 27. 298-318.
478 10.1190/1.2896620, 2008.

479 Ciaccio, M., Barchi M. R., Chiarabba, C., Mirabella, F. and Stucchi E.: Seismological, geological and geophysical constraints
480 for the Gualdo Tadino fault, Umbria-Marche Apennines (central Italy), Tectonophysics, 406, 233 – 247, 2005.

481 Civico, R., Pucci, S., Villani, F., Pizzimenti, L., De Martini, P. M., Nappi, R. & the Open EMERGEO Working Group: Surface
482 ruptures following the 30 October 2016 Mw 6.5 Norcia earthquake, central Italy, Journal of Maps, 14:2, 151-160, doi:
483 10.1080/17445647.2018.1441756, 2018.

484 Coltorti, M., Farabollini, P.: Quaternary evolution of the "Castelluccio di Norcia" basin (Umbro-Marchean Apennines, central
485 Italy). Il Quaternario 8(1), 149–166, 1995.

486 Cook, F. A., Albaugh, D. S., Brown, L. D., Kaufman, S., Oliver, J. E., & Hatcher Jr, R. D.: Thin-skinned tectonics in the
487 crystalline southern Appalachians; COCORP seismic-reflection profiling of the Blue Ridge and Piedmont. Geology, 7(12),
488 563-567, 1979.

489 De Guidi, G., Vecchio, A., Brighenti, F., Caputo, R., Carnemolla, F., Di Pietro, A., et al.: Co-seismic displacement on October
490 26 and 30, 2016 (Mw 5.9 and 6.5) earthquakes in central Italy from the analysis of discrete GNSS network. Natural Hazards
491 and Earth System Sciences Discussions, 2017(May), 1–11. doi: 10.5194/nhess-2017-130, 2017.

492 Deschamps, A., Innaccone, G., & Scarpa, R.: The Umbrian earthquake (Italy) of 19 September 1979. Annales Geophysicae,
493 2, 29–36, 1984.

494 De Lima, R. & Luiz Evangelista Teixeira, W. & Ramos de Albuquerque, F. & Lima-Filho, F. P.: Ground Penetrating Radar
495 digital imaging and modeling of microbialites from the Salitre Formation, Northeast Brazil. Geologia USP - Serie Cientifica,
496 18, 187-200. doi: 10.11606/issn.2316-9095.v18-146075, 2018.

497 Di, H., and AlRegib, G.: Semi-automatic fault/fracture interpretation based on seismic geometry analysis: Geophysical
498 Prospecting, doi: 10.1111/1365-2478.12769, 2019.

499 DISS Working Group: Database of Individual Seismogenic Sources (DISS), Version 3.2.1: A compilation of potential sources
500 for earthquakes larger than M 5.5 in Italy and surrounding areas. http://diss.rm.ingv.it/diss/, Istituto Nazionale di Geofisica e
501 Vulcanologia, doi: 10.6092/INGV.IT-DISS3.2.1, 2018.

502 Ercoli, M., Pauselli, C., Frigeri, A., Forte, E., & Federico, C.: "Geophysical paleoseismology" through high resolution GPR
503 data: A case of shallow faulting imaging in Central Italy. Journal of Applied Geophysics, 90, 27–40.
504 doi.org/10.1016/j.jappgeo.2012.12.001, 2013.

505 Ercoli M., Pauselli C., Frigeri A., Forte E. and Federico C.: 3-D GPR data analysis for high-resolution imaging of shallow
506 subsurface faults: the Mt Vettore case study (Central Apennines, Italy). Geophysical Journal International, 198:1(609-621).
507 doi: 10.1093/gji/ggu156, 2014.

508 Ercoli, M., Pauselli, C., Cinti, F.R., Forte, E. and Volpe, R.: Imaging of an active fault: Comparison between 3D GPR data
509 and outcrops at the Castrovillari fault, Calabria, Italy. Interpretation, 3(3), pp. SY57-SY66, 2015.

510 Ferrario, M. F., & Livio, F.: Characterizing the distributed faulting during the 30 October 2016, Central Italy earthquake: A
511 reference for fault displacement hazard assessment. Tectonics, 37, 1256–1273. https://doi.org/10.1029/2017TC004935, 2018.

512 Finetti, I. R., Boccaletti, M., Bonini, M., Del Ben, A., Geletti, R., Pipan, M., & Sani, F.: Crustal section based on CROP seismic
513 data across the North Tyrrhenian–Northern Apennines–Adriatic Sea. Tectonophysics, 343(3-4), 135-163, 2001.

514 Ferrario, M. F., & Livio, F.: Characterizing the distributed faulting during the 30 October 2016, Central Italy earthquake: A
515 reference for fault displacement hazard assessment. Tectonics, 37. doi:10.1029/2017TC004935, 2018.

516 Forte E., Pipan M., Casabianca D., Di Cuia R., Riva A.: Imaging and characterization of a carbonate hydrocarbon reservoir
517 analogue using GPR attributes. Journal of Applied Geophysics, 81, 76–87, 2012.

518 Forte E., Dossi M., Pipan M. and Del Ben A.: Automated phase attribute-based picking applied to reflection seismics,
519 Geophysics, 81, 2, V55-V64, doi: 10.1190/GEO2015-0333.1, 2016.

520 Galadini, F., & Galli, P.: Paleoseismology of silent faults in the central Apennines (Italy): The Mt. Vettore and Laga Mts.
521 Faults. Annals of Geophysics, 46. https://doi.org/10.4401/ag-3457, 2003.

522 Galadini, F., Falcucci, E., Gori, S., Zimmaro, P., Cheloni, D. and Stewart J. P.: Active Faulting in Source Region of 2016–
523 2017 Central Italy Event Sequence. Earthquake Spectra, 34, 4, 1557-1583, 2018.

524 Galli, P., Galadini, F., Calzoni, F.: Surface faulting in Norcia (Central Italy): a "paleoseismological perspective".
525 Tectonophysics, 403, 117–130, 2005.

526 Galli, P., Galadini, F. & Pantosti, D.: Twenty years of paleoseismology in Italy, Earth-Sci. Rev., 88(1–2), 89–117, 2008.

527 Galli, P., Galderisi, A., Ilardo, I., Piscitelli, S., Scionti, V., Bellanova, J., Calzoni, F.: Holocene paleoseismology of the Norcia
528 fault system (Central Italy), Tectonophysics, 745, 154-169, doi:10.1016/j.tecto.2018.08.008, 2018.

529 Gruppo di Lavoro Sequenza Centro Italia: Rapporto Bollettino Sismico Italiano sulla revisione dei giorni 24-26 agosto; 26-27
530 ottobre; 30 ottobre - 1° novembre 2016. Bollettino Sismico Italiano (BSI), 13 pp., 2019.

531 Jibson, R.W., Allstadt, K.E., Rengers, F.K., and Godt, J.W.: Overview of the geologic effects of the November 14, 2016, Mw
532 7.8 Kaikoura, New Zealand earthquake, U.S. Geological Survey Scientific Investigations Report, 2017–5146, 39 pp.,
533 https://doi.org/10.3133/sir20175146, 2018.

534 Ha, T. N., Marfurt, K. J. and Wallet B. C., Hutchinson, B.: Pitfalls and implementation of data conditioning, attribute analysis,
535 and self-organizing mapping to 2D data: Application to the Exmouth Plateau, North Carnarvon Basin, Australia, Interpretation,
536 submitted, http://mcee.ou.edu/aaspi/submitted/2019/Ha_et_al_2019_Seismic_attributes_for_2D_data.pdf, 2019.

537 Hale, D.: Methods to compute fault images, extract fault surfaces, and estimate fault throws from 3D seismic images.
538 Geophysics, 78(2), O33–O43, https://doi.org/10.1190/geo2012-0331.1, 2013.

539 Hutchinson, B.: Application and Limitations of Seismic Attributes on 2D Reconnaissance Surveys: Master's thesis, University
540 of Oklahoma, 130 pp., 2016. https://shareok.org/handle/11244/34658.

541 Improta, L., Latorre, D., Margheriti, L., Nardi, A., Marchetti, A., Lombardi, A. M., Castello, B., Villani, F., Ciaccio, M. G.,
542 Mele, F. M., Moretti, M. & the Bollettino sismico Italiano Working Group: Multi-segment rupture of the 2016 Amatrice-
543 Visso-Norcia seismic sequence (central Italy) constrained by the first high-quality catalog of early Aftershocks. Scientific
544 Reports, 9, 6921, 2019. doi: 10.1038/s41598-019-43393-2

545 ISIDe working group: version 1.0; doi:10.13127/ISIDe, 2016.

546 Ithaca catalogue, Available at: http://www.isprambiente.gov.it/it/progetti/ suolo-e-territorio-1/ithaca-catalogo-delle-faglie-
547 capaci, last accessed January 2019.

548 Koopman, A.: Detachment tectonics in the central Apennines, Italy. Geologica Eltraiectina, 30, 1–155, 1983.

549 Lavecchia, G.: Il sovrascorrimento dei Monti Sibillini: Analisi cinematica e strutturale. Bollettino della Società Geologica
550 Italiana, 104, 161–194, 1985.

551 Lavecchia, G., Brozzetti, F., Barchi, M., Keller, J., & Menichetti, M.: Seismotectonic zoning in east-central Italy deduced from
552 the analysis of the Neogene to present deformations and related stress fields. Geological Society of America Bulletin, 106,
553 1107–1120, 1994.

554 Lavecchia, G., Castaldo, R., de Nardis, R., De Novellis, V., Ferrarini, F., Pepe, S., Brozzetti, F., Solaro, G., Cirillo, D., Bonano,
555 M., Boncio, P., Casu, F., De Luca, C., Lanari, R., Manunta, M., Manzo, M., Pepe, A., Zinno, I., Tizzani, P.: Ground

556 deformation and source geometry of the 24 August 2016 Amatrice earthquake (Central Italy) investigated through analytical

557 and numerical modeling of DInSAR measurements and structural-geological data. Geophysical Research Letters, 43, 12,389–

558 12,398 American Geophysical Union (AGU), 2016.

559 Lima, R. & Teixeira, L. E. W., de Albuquerque, F. R., and Lima-Filho, F. (2018). Ground Penetrating Radar digital imaging

560 and modeling of microbialites from the Salitre Formation, Northeast Brazil. Geologia USP - Serie Cientifica. 18. 187-200.

561 10.11606/issn.2316-9095.v18-146075.

562 Livio, F., Michetti, A. M., Vittori, E., Gregory, L., Wedmore, L., Piccardi, L., et al.: Surface faulting during the August 24,

563 2016, central Italy earthquake (Mw 6.0): Preliminary results. Annals of Geophysics, 59. doi: 10.4401/ag-7197, 2016.

564 Maesano, F. E., D'Ambrogi, C., Burrato, P., & Toscani, G.: Slip-rates of blind thrusts in slow deforming areas: examples from

565 the Po Plain (Italy). Tectonophysics, 643, 8-25, 2015.

566 Mancinelli, P., Porreca, M., Pauselli, C., Minelli, G., Barchi, M. R., & Speranza, F.: Gravity and magnetic modeling of Central

567 Italy: Insights into the depth extent of the seismogenic layer. Geochemistry, Geophysics, Geosystems, 20, 2019,

568 https://doi.org/10.1029/2018GC008002.

569 Marfurt, K. J. Gao, D., Barnes, A., Chopra, S., Corrao, A., Hart, B., James, H., Pacht, J., Rosen, N.C.: SEPM Society for

570 Sedimentary Geology, 31, doi: 10.5724/gcs.11.31, 2011.

571 Marfurt, K. J.: Seismic Attributes as the Framework for Data Integration throughout the Oilfield Life Cycle, SEG, 508 pp.,

572 2018.

573 Martinis, B., and Pieri, M.: Alcune notizie sulla formazione evaporitica dell'Italia centrale e meridionale. Bollettino della

574 Società Entomologica Italiana, 4, 649–678, 1964.

575 Mazzotti, A., Stucchi, E., Fradelizio, G., Zanzi, L., Scandone, P.: Seismic exploration in complex terrains: A processing

576 experience in the southern Apennines. Geophysics, 65(5), 1402–1417. https://doi.org/10.1190/1.1444830, 2000.

577 McClymont, A. F., Green, A. G., Villamor, P., Horstmeyer, H., Grass, C. and Nobes, D. C.: Characterization of the shallow

578 structures of active fault zones using 3-D ground-penetrating radar data, J. Geophys. Res., 113, B10315,

579 doi:10.1029/2007JB005402, 2008.

580 Milli, S., Moscatelli, M., Stanzione, O., & Falcini, F.: Sedimentology and physical stratigraphy of the Messinian turbidites

581 deposits of the Laga basin (Central Apennines, Italy). Bollettino della Società Geologica Italiana, 126, 37–48, 2007.

582 Minelli, G., and Menichetti, M.: Tectonic evolution of the Perugia massifs area (Central Italy). Bollettino della Società

583 Entomologica Italiana, 109(5), 445–453, 1990.

584 Mirabella, F., Barchi, M. R. and Lupattelli, A.: Seismic reflection data in the Umbria Marche region: Limits and capabilities

585 to unravel the subsurface structure in a seismically active area. Annals of Geophysics, 51(2–3), 383–396.

586 https://doi.org/10.4401/ag-3032, 2008.

587 Naeini E. Z. and Prindle, K.: Machine learning and learning from machines, The Leading Edge, 37:12, 886-893, 2018.

588 Patacca, E., and Scandone, P.: Late thrust propagation and sedimentary response in the thrust-belt foredeep system of the
589 southern Apennines (Pliocene–Pleistocene). In G. Vai & I. Martini (Eds.), Anatomy of an Orogen: The Apennines and adjacent
590 Mediterranean basins, 441–454, Norwell, MA: Kluwer Acad., 2001.

591 Pauselli, C., Barchi, M. R., Federico, C., Magnani, M. B. and Minelli, G.: The crustal structure of the northern Apennines
592 (Central Italy): An insight by the CROP03 seismic line. American Journal of Science, 306(6), 428–450.
593 https://doi.org/10.2475/06.2006.02, 2006.

594 Pauselli, C., Federico, C., Frigeri, A., Orosei, R., Barchi, M.R. & Basile, G.: Ground Penetrating Radar investigations to study
595 active faults in the Norcia Basin (Central Italy), Journal of Applied Geophysics, 72, 39-45, 2010.

596 Pierantoni, P. P., Deiana, G., & Galdenzi, S.: Stratigraphic and structural features of the Sibillini Mountains (Umbria–Marche
597 Apennines, Italy). Italian Journal of Geosciences, 132, 497–520. https://doi.org/10.3301/IJG.2013.08, 2013.

598 Pizzi, A., Calamita, F., Coltorti, M., & Pieruccini, P.: Quaternary normal faults, intramontane basins and seismicity in the
599 Umbria-MarcheAbruzzi Apennine Ridge (Italy): Contribution of neotectonic analysis to seismic hazard assessment. Bollettino
600 Società Geologica Italiana Special Publication, 1(January), 923–929, 2002.

601 Porreca, M., Minelli, G., Ercoli, M., Brobia, A., Mancinelli, P., Cruciani, F., Giorgetti, C., Carboni, C., Mirabella, F., Cavinato,
602 G., Cannata, A., Pauselli, C., Barchi, M.R.: Seismic reflection profiles and subsurface geology of the area interested by the
603 2016–2017 earthquake sequence (Central Italy). Tectonics, 37, 1-22, doi: 10.1002/2017TC004915, 2018.

604 Press, F., and D. Jackson: Alaskan earthquake, 27 March 1964: Vertical extent of faulting and elastic strain energy release,
605 Science, 147, 867, 1965.

606 Pucci, S, De Martini, P.M., Civico, R., Villani, F, Nappi, R., Ricci, T., Azzaro, R., Brunori, C. A., Caciagli, M., Cinti, F. R.,
607 Sapia, V., De Ritis, R., Mazzarini, F., Tarquini, S., Gaudiosi, G., Nave, R., Alessio, G., Smedile, A., Alfonsi, L., Cucci, L.,
608 Pantosti. D.: Coseismic ruptures of the 24 August 2016, Mw6.0 Amatrice earthquake (central Italy). Geophysical Research
609 Letters, American Geophysical Union (AGU), 2017.

610 Ramsay, J. G., Huber, M. I.: The Techniques of Modern Structural Geology: Folds and Fractures. Elsevier Science, 391 pp.,
611 1987.

612 Roure, F., P. Choukroune, X. Berastegui, J. A. Munoz, A. Villien, P. Matheron, M. Bareyt, M. Seguret, P. Camara, and J.
613 Deramond: Ecors deep seismic data and balanced cross sections: Geometric constraints on the evolution of the Pyrenees,
614 Tectonics, 8(1), 41–50, doi:10.1029/TC008i001p00041, 1989.

615 Rovida, A., Locati, M., Camassi, R., Lolli, B., & Gasperini P. (Eds.): CPTI15, the 2015 version of the parametric catalogue of
616 Italian earthquakes, Istituto Nazionale di Geofisica e Vulcanologia. https://doi.org/10.6092/INGV.IT-CPTI15, 2016.

617 Schwartz, D. P., & Coppersmith, K. J.: Fault behavior and characteristic earthquakes: Examples from the Wasatch and San
618 Andreas fault zones. Journal of Geophysical Research: Solid Earth, 89(B7), 5681-5698, 1984.

619 Serva L., Blumetti A.M., Guerrieri L. and Michetti A.M.: The Apennine intermountain basins: the result of repeated strong
620 earthquakes over a geological time interval. Boll. Soc. Geol. It., 1, 939-946, 2002.

621 Simancas, J. F., Carbonell .R., González Lodeiro, F., Pérez Estaún, A., Juhlin, C., Ayarza, P., Kashubin, A., Azor, A., Martínez
622 Poyatos, D., Almodóvar, G.R., Pascual, E., Sáez, R., Expósito, I.: Crustal structure of the transpressional Variscan orogen of
623 SW Iberia: SW Iberia deep seismic reflection profile (IBERSEIS), *Tectonics*, 22, 1062, doi:10.1029/2002TC001479, 6, 2003.

624 Taner, M.T., Koehler, F., and Sheriff, R.E.: Complex Seismic Trace Analysis. Geophysics, 44 (6): 1041.
625 http://dx.doi.org/10.1190/1.1440994, 1979.

626 Taner, M.T.: Seismic attributes. Canadian Society of Exploration Geophysicists Recorder, 26. 48-56, 2001.

627 Tarquini, S., Isola, I., Favalli, M., & Boschi, E.: TINITALY/01: a new triangular irregular network of Italy. Annals of
628 Geophysics, 50–53, 2007.

629 Tarquini, S., Vinci, S., Favalli, M., Doumaz, F., Fornaciai, A., & Nannipieri, L.: Release of a 10-m-resolution DEM for the
630 Italian territory: Comparison with global-coverage DEMs and anaglyph-mode exploration via the web. Computers and
631 Geosciences, 38(1), 168–170. https://doi.org/10.1016/j.cageo.2011.04.018, 2012.

632 Trippetta, F., Collettini, C., Vinciguerra, S., & Meredith, P. G.: Laboratory measurements of the physical properties of Triassic
633 evaporites from Central Italy and correlation with geophysical data. Tectonophysics, 492(1), 121–132, 2010.

634 Torvela T., Moreau, J., Butler, R., W. H, Korja, A. and Heikkinen, P.: The mode of deformation in the orogenic mid-crust
635 revealed by seismic attribute analysis, Geochem., Geophys., Geosyst., 14, 1069–1086, 2013.

636 Vai, G. B.: Basement and early (pre-Alpine) history. In G. B. Vai & I. P. Martini (Eds.), Anatomy of an orogen: The Apennines
637 and adjacent Mediterranean basins, 121–150, Dordrecht, Netherlands: Kluwer Academic Publisher.
638 https://doi.org/10.1007/978-94-015-9829-3_10, 2001.

639 Valoroso, L. et al. Radiography of a normal fault system by 64,000 high-precision earthquake locations: The 2009 L'Aquila
640 (central Italy) case study. J. Geophys. Res. - Solid Earth, 118, 1156–1176, https://doi.org/10.1002/jgrb.50130, 2013.

641 Vernengo, L., Trinchero, E., Torrejón, M. G., and Rovira, I.: Amplitude volume technique attributes and multidimensional
642 seismic interpretation. The Leading Edge, 36(9), 776–781. https://doi.org/10.1190/tle36090776.1, 2017.

643 Villani, F., Pucci, S., Civico, R., De Martini, P. M., Cinti, F. R., & Pantosti, D.: Surface faulting of the 30 October 2016 Mw
644 6.5 central Italy earthquake: Detailed analysis of a complex coseismic rupture. Tectonics, 37, 3378–3410.
645 https://doi.org/10.1029/2018TC005175, 2018a.

646 Villani, F., Sapia, V., Baccheschi, P., Civico, R., Di Giulio, G., Vassallo, M., et al.: Geometry and structure of a fault bounded
647 extensional basin by integrating geophysical surveys and seismic anisotropy across the 30 October 2016 Mw 6.5 earthquake
648 fault (central Italy): The Pian Grande di Castelluccio basin. Tectonics, 37. https://doi.org/10.1029/2018TC005205, 2018b.

649 Yi, S., Wu, C., Li, Y. et al. J. Mt. Sci.: Source tectonic dynamics features of Jiuzhaigou Ms 7.0 earthquake in Sichuan Province,
650 China, Journal of Mountain Science, 15(10): 2266-2275. doi: 10.1007/s11629-017-4703-6, 2018.

651 Wilkinson, M. W., McCaffrey, K. J. W., Jones, R. R., Roberts, G. P., Holdsworth, R. E., Gregory, L. C., et al.: Near-field fault
652 slip of the 2016 Vettore Mw 6.6 earthquake (Central Italy) measured using low-cost GNSS. Scientific Reports, 7(1), 4612,
653 doi:10.1038/s41598- 017-04917-w, 2017.

654 Wrona, T., Pan, I., Gawthorpe, R. L. and Fossen, H.: Seismic facies analysis using machine learning, Geophysics, 83:5, O83-
655 O95, 2018.

656 Wyss, M. and Brune, J. N.: The Alaska earthquake of 28 March 1964: A complex multiple rupture, Bull. Seism. Soc. Amer.
657 57, (5), 1967.

658 Zhao, W., Forte, E., Fontolan, G., Pipan, M.: Advanced GPR imaging of sedimentary features: integrated attribute analysis
659 applied to sand dunes, Geophysical Journal International, 213:1, 147–156, https://doi.org/10.1093/gji/ggx541, 2018.
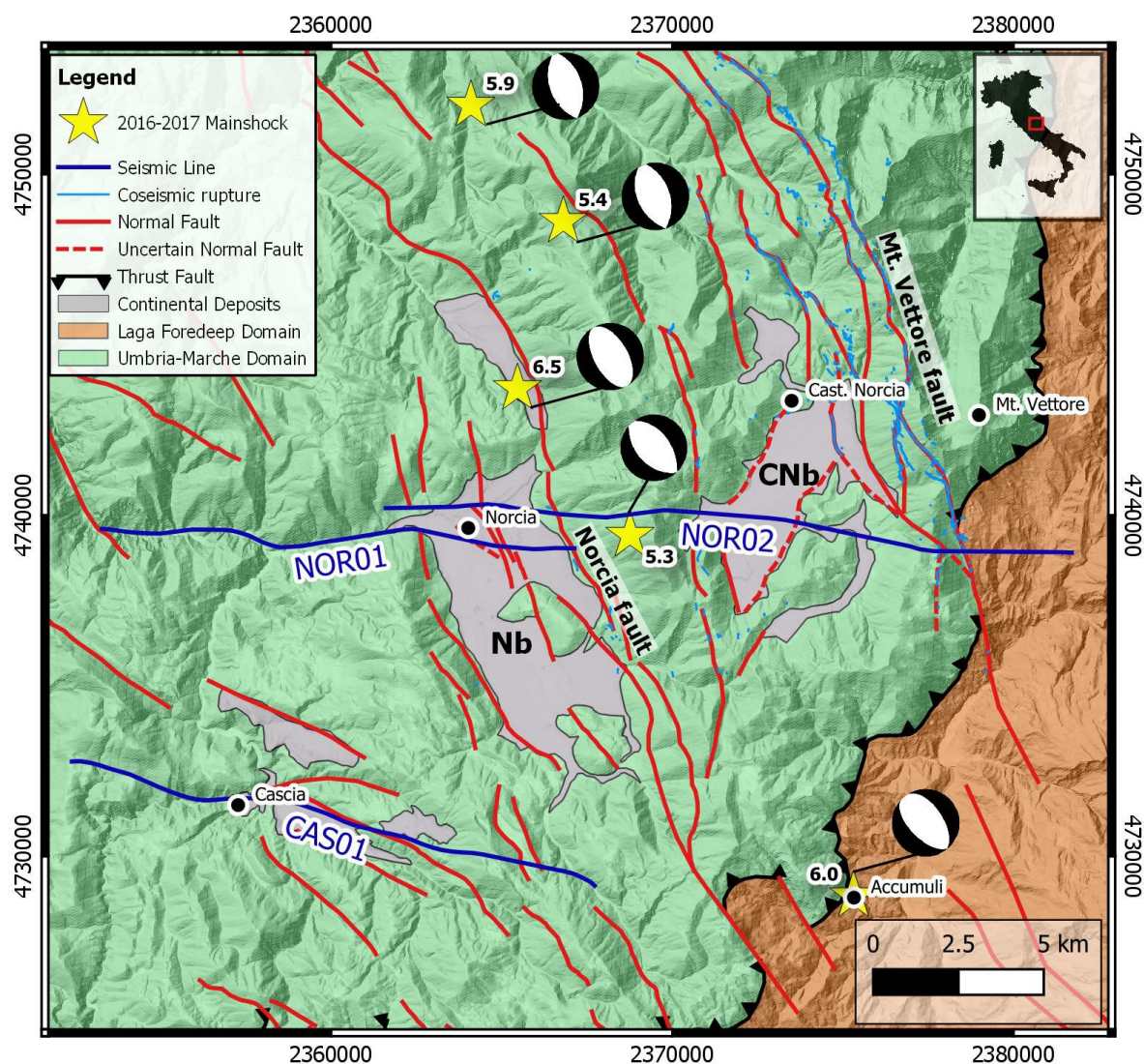
660 ---

661 **Figure 1**

662

663

Figure 2

Figure 3

Figure 4

666

Figure 5

Figure 6

670

671

Figure 7

672

673

674
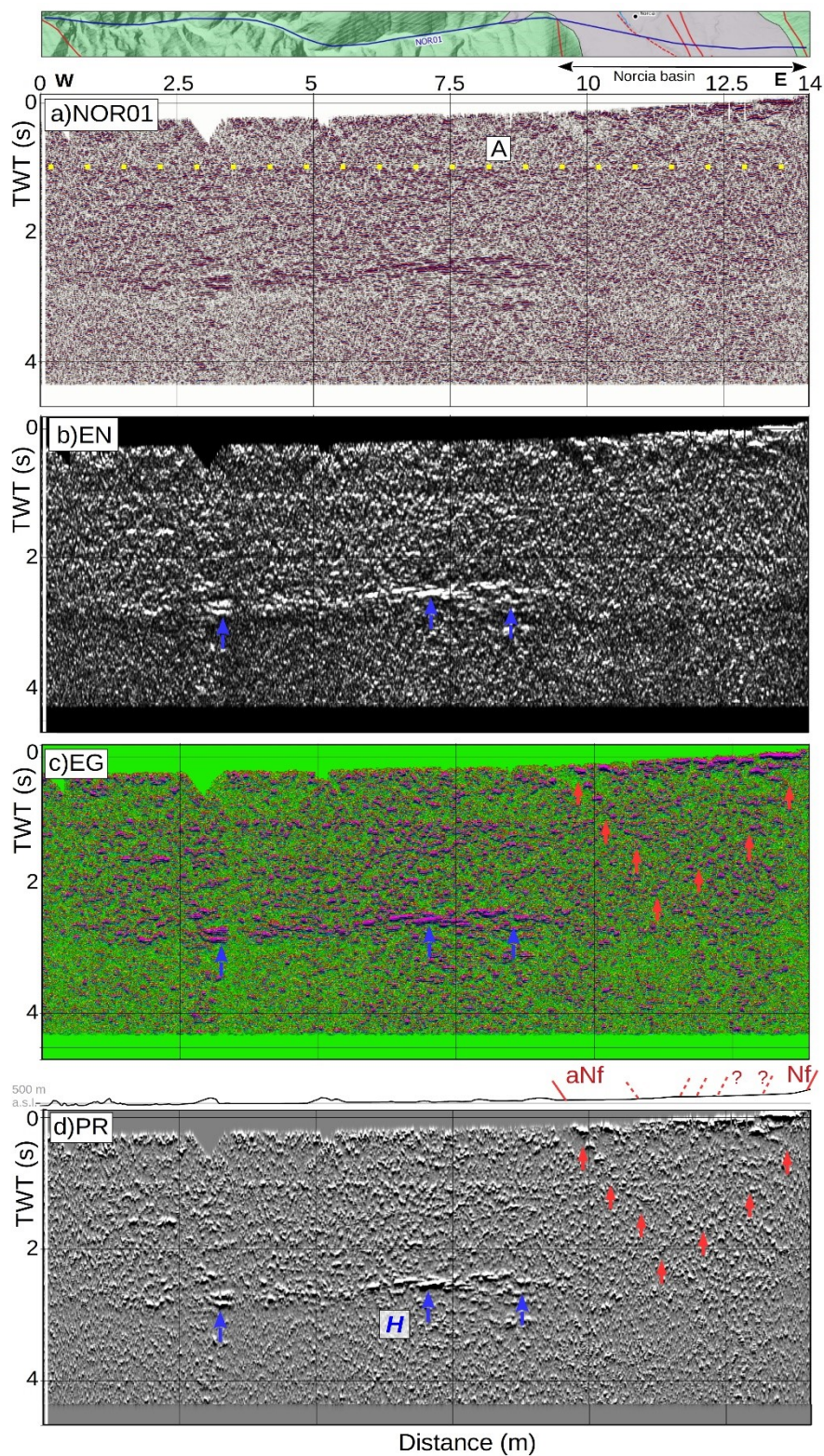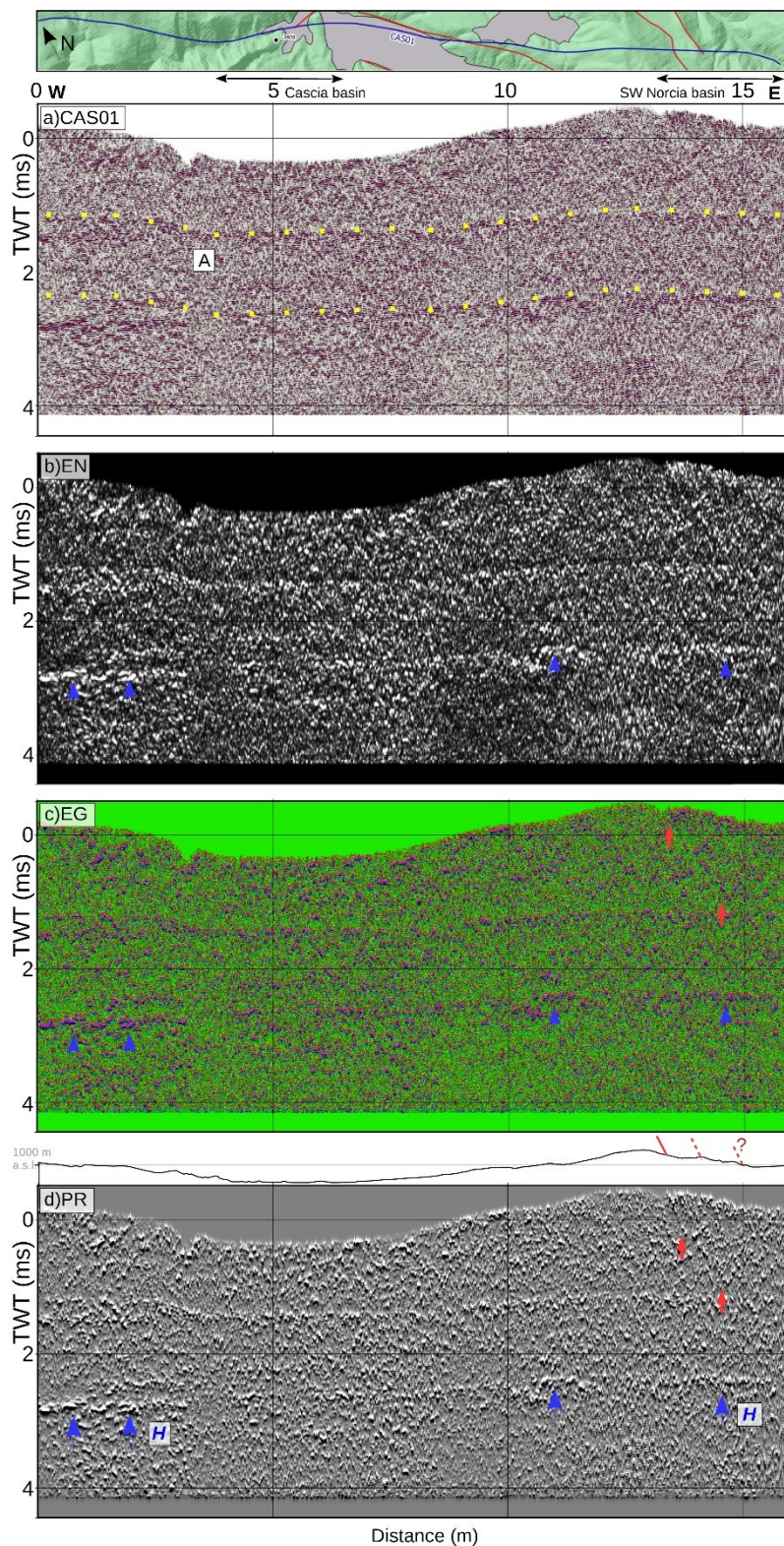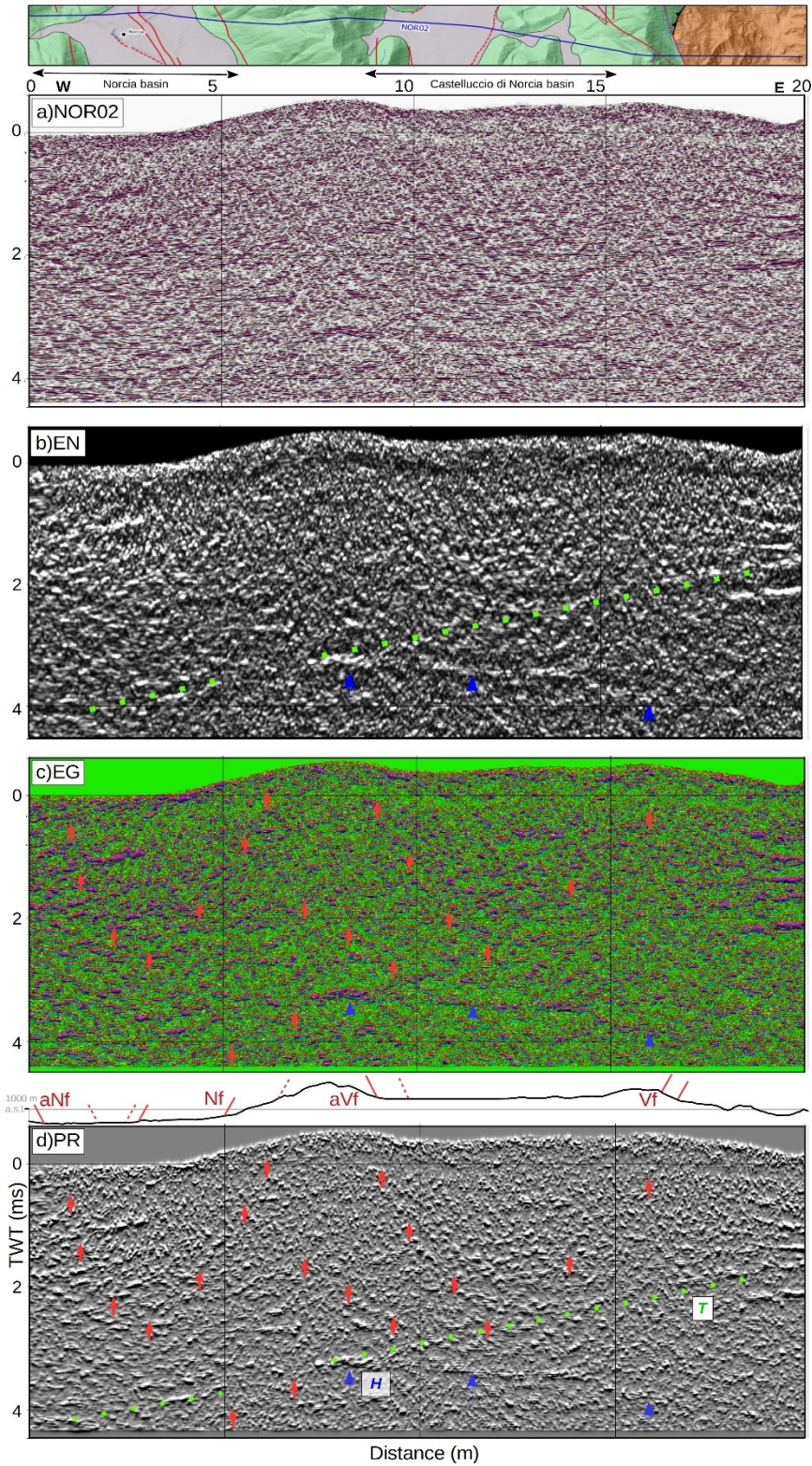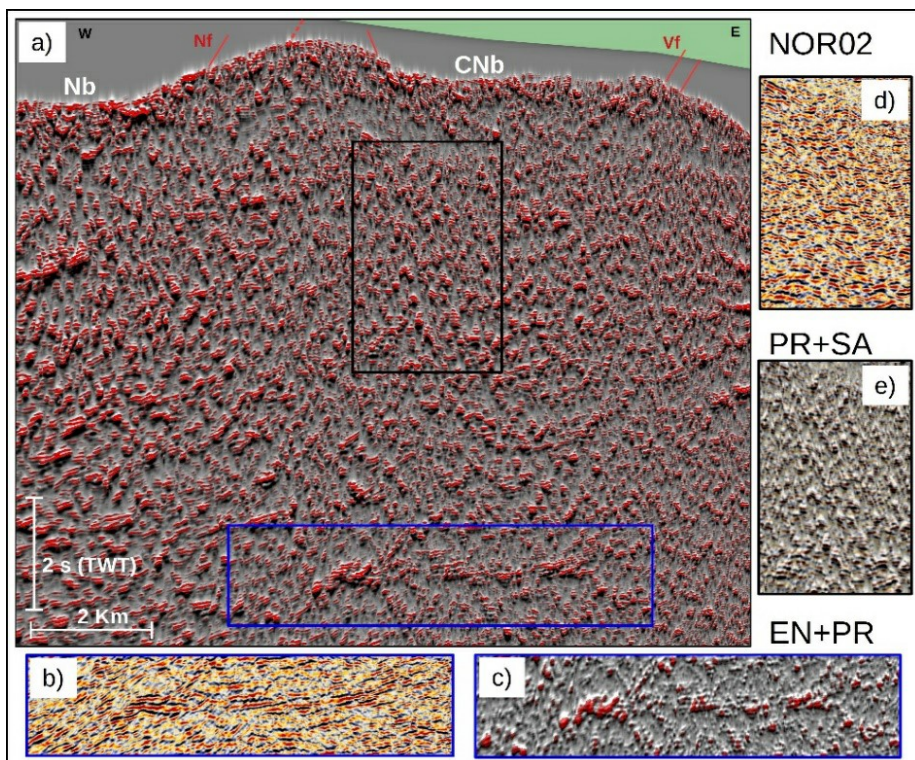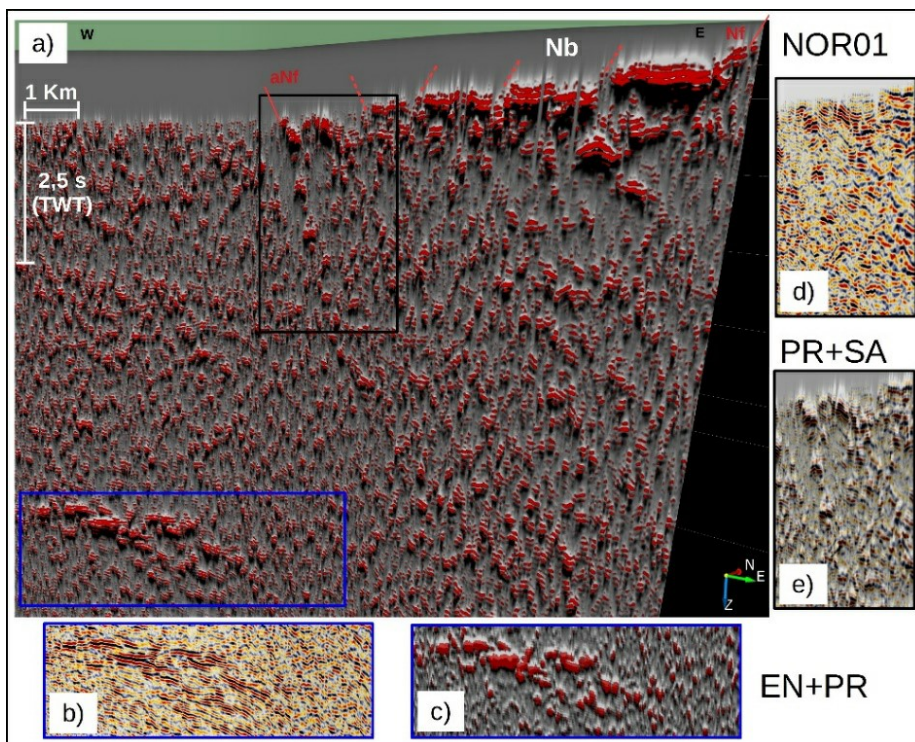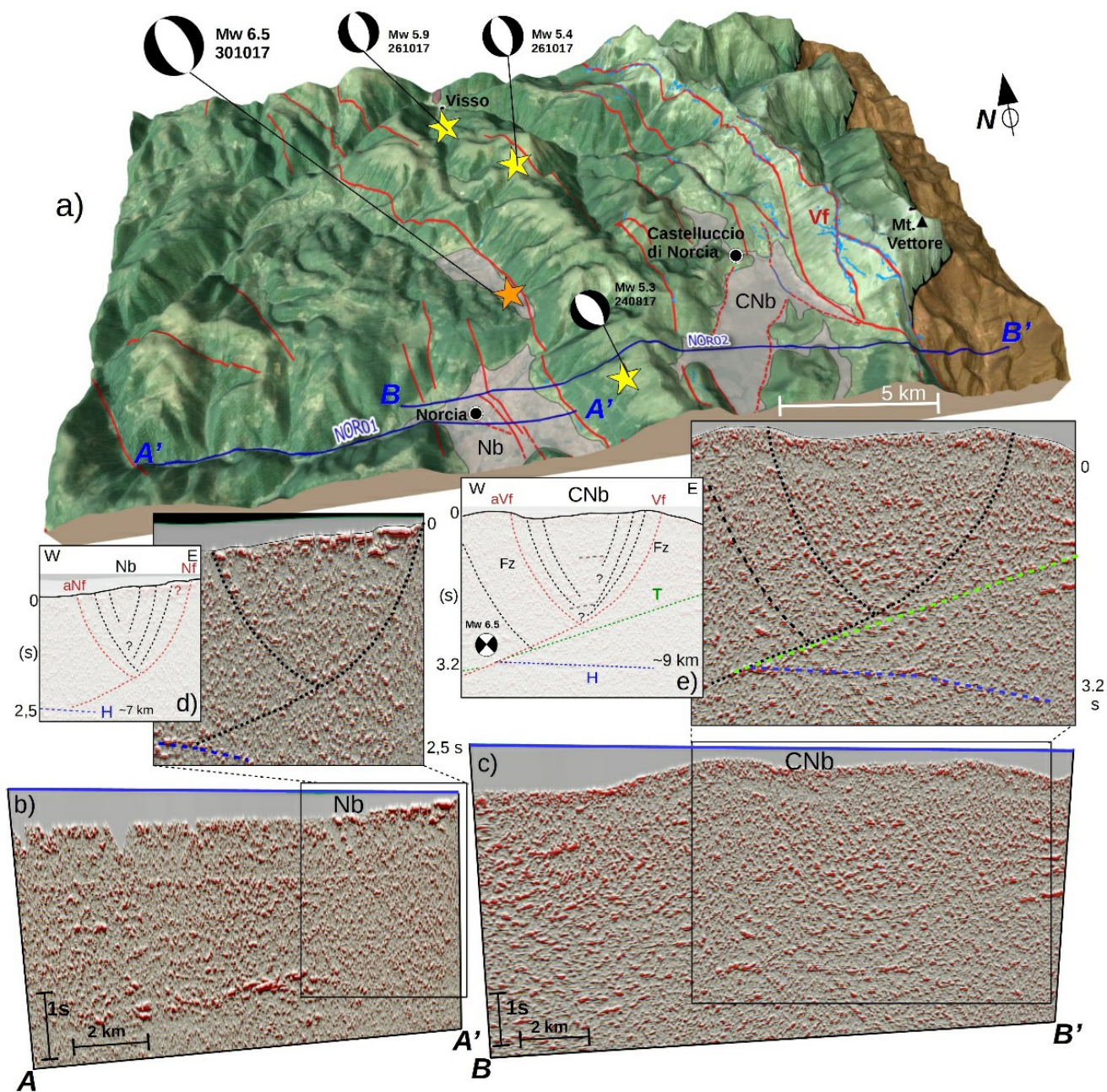
675   **Table 1**

Parameters	NOR01	NOR02	CAS01
Source	Vibroseis	Vibroseis	Explosive
Length (km)	14	20	16
Number of traces	938	825	1069
Samples/trace	1600	1750	1600
Time window (ms)	6400	7000	6400
Sampling interval (ms)	4	4	4
Trace interval (m)	15	25	15
Mean Spectral amplitude (dB)			

676

677   **Figures and Tables captions:**

678   **Figure 1: Simplified geological map of the study area (modified after Porreca et al., 2018), showing the 2D seismic data tracks, the**
679   **2016-2017 mainshock locations, beachballs and magnitudes, the surface ruptures and the known master faults. Nb Norcia basin,**
680   **CNb Castelluccio di Norcia basin.**

681   **Figure 2: Stack version of NOR01; a) reflection amplitude, yellow dots underline a processing artefact (A); b) Energy attribute**
682   **enhancing a strong reflectivity contrasts (H, blue arrows); c) Energy Gradient, improving the detection of dipping alignments and**
683   **continuity of reflectors; d) Pseudo-Relief enhancing the reflection patterns cross-cut by steep discontinuities (red arrows). Nf Norcia**
684   **fault, aNf antithetic Norcia fault.**

685   **Figure 3: Stack version of CAS01, with same attributes computation: a) reflection amplitude (yellow dots display processing**
686   **artefacts); b) Energy attribute c) Energy Gradient attribute; d) Pseudo-Relief, showing the strong regional reflector H (blue arrows).**
687   **A high-angle discontinuity on the western margin is interpretable as a normal fault, showing an attribute signature analogous to**
688   **aNf.**

689   **Figure 4: Time migrated version of NOR02; a) reflection amplitude; b) Energy attribute displaying the reflector H (blue arrows)**
690   **and a possible low angle discontinuity (T, green dots); c) Energy Gradient attribute, showing the master faults bounding the basins**
691   **(red arrows); d) Pseudo-Relief, improving the reflectors continuity/discontinuity and the master faults display (red arrows). Nf**
692   **Norcia fault, aNf antithetic Norcia fault; Vf Mt. Vettore fault, aVf antithetic Mt. Vettore fault.**

693   **Figure 5: Multi-attribute display of NOR02; a) EN+PR attributes, the seismic facie in the blue box is compared with the original**
694   **seismic line (b) and EN+PR (c) for comparison; the same plot for the black box is reported in figures d) and e) (original line and**
695   **PR+SA, respectively).**

696   **Figure 6: Multi-attribute display of NOR01; a) EN+PR attributes, the seismic facie in the blue box showing a strong set of deep**
697   **reflectors is compared with the original seismic line in b) and EN+PR c). An analogous plot of the black box reports in figures d)**
698   **and e) the original line and the combination PR+SA.**

699   **Figure 7: Integration of surface and subsurface data (DTM by Tarquini et al., 2012); a) 3D-view of a W-E section crossing Nb and**
700   **CNb, and the mainshock locations (ISIDe working group, 2016). Surface and deep data allow to correlate the master faults and**
701   **coseismic ruptures at the surface. The multi-attribute display of NOR01 (b) and NOR02 (c), is obtained overlapping the reflection**
702   **amplitude in transparency with the Pseudo-Relief and Energy attributes (red palette). A significative improvement of the subsurface**
703   **images provides unprecedent details on the seismogenic fault zones: the two conjugate basins show master faults along the borders**
704   **and some minor synthetic and antithetic splays (see d) and e) sketches).**

705   **Table 1: List of some parameters extracted from SEG-Y headers and three mean frequency spectra of the three seismic lines. An**
706   **approximate vertical resolution equal to 80 m was derived (v=6 km/s).**